

Controlled preparation of ZnS nanoparticle arrays in Langmuir monolayer of an unsymmetrical phthalocyaninato zinc complex: Synthesis, organization and semiconducting properties

Kai Chen^{a‡}, Yanling Wu^{a‡}, Xia Kong^b, Pingshun Zhang^a, Feifei Sun^a, Yanli Chen^{*a,b,δ} and Jianzhuang Jiang^{*b,c,δ}

^aShandong Provincial Key Laboratory of Fluorine Chemistry and Chemical Materials, School of Chemistry and Chemical Engineering, University of Jinan, Jinan 250022, China

^bSchool of Science, China University of Petroleum (East China), Qingdao 266580, China

^cBeijing Key Laboratory for Science and Application of Functional Molecular and Crystalline Materials, Department of Chemistry, University of Science and Technology Beijing, Beijing 100083, China

Dedicated to Professor Tomás Torres on the occasion of his 65th birthday

Received 22 March 2016

Accepted 9 May 2016

ABSTRACT: A new unsymmetrical phthalocyaninato zinc complex with typical amphiphilic nature, namely 2,3-di(4-hydroxyphenoxy)-9,10,16,17,24,25-hexakis(*n*-octyloxy)phthalocyaninato zinc, Zn[Pc(OC₈H₁₇)₆(OPhOH)₂], has been designed, synthesized, and characterized by a range of spectroscopic methods. The Langmuir monolayer of this amphiphilic complex has been used as not only an organic template but also as a good functional organic material to produce the monodispersed nanoparticles of Zn[Pc(OC₈H₁₇)₆(OPhOH)₂]/ZnS nanocomposite. In addition, multilayer pure and hybrid films have also been obtained by depositing monolayers of the amphiphilic complex and Zn[Pc(OC₈H₁₇)₆(OPhOH)₂]/ZnS nanocomposite, respectively, using the Langmuir–Shäfer (LS) method. Surface pressure-area isotherms, UV-vis spectroscopic, and XRD studies indicate that the molecules adopted a face-to-face configuration and edge-on orientation in both the multilayer pure LS and Zn[Pc(OC₈H₁₇)₆(OPhOH)₂]/ZnS hybrid films. In particular, current–voltage (*I*–*V*) measurements reveal the superior conductivity of the Zn[Pc(OC₈H₁₇)₆(OPhOH)₂]/ZnS hybrid film nanocomposites to that of the stand-alone films, and this is due to the existence of the densely packed molecular architecture in the film matrix and the large interfacial area between the two components. These characteristics remove the charge transporting bottleneck by creating an interpenetrating consistent thin film of hybrid materials. The result sheds lights on new ways for developing organic-inorganic hybrid nanostructures with good semiconducting properties.

KEYWORDS: unsymmetrical phthalocyanine, ZnS, organic-inorganic nanocomposite, conductivity.

^δSPP full member in good standing

*Correspondence to: Yanli Chen, email: chm_chenyl@ujn.edu.cn, fax: +86 (0)531-8973-6150; Jianzhuang Jiang, email: jianzhuang@ustb.edu.cn, fax: +86 (0)10-6233-2462

[‡]These authors contributed equally to this work.

INTRODUCTION

Organic/inorganic nanocomposite materials have been widely recognized as one of the most promising and rapidly emerging research areas for advanced materials due to their desirable optical, electrical, and magnetic

properties [1–7]. The combined unique properties offered by both organic and inorganic components on a nanoscale level make such nanocomposites attractive for an extensive range of applications including next generation optics, optoelectronic nano-devices, thin-film field-effect transistors, chemical or biological sensors and catalysts [8]. Many organic/inorganic hybrid nanostructure films of CdSe, CdS, TiO₂, Au, ZrO₂ and MoS₂ have been fabricated depending on hydrogen bonding, van der Waals contacts, and/or electrostatic interactions between organic and inorganic components [8, 9]. Quite recently, growing of inorganic nanostructures directly on the organic template by controlled modification of interface has attracted considerable research interest as a new and facile approach to fabricate semiconducting nanostructures [8–13]. For example, the twisted nanoribbons of ethyl methacrylate were employed as the template for preparing helical cadmium sulfide (CdS) semiconductor [14]. The patterned self-assembled monolayers of alkanethiolates on gold were used as the template to prepare the cube-shaped CdS nanoparticles [15]. In addition, an aminopyrene-modified carbon nanotube has also been served as an excellent template to fabricate the nanoscale CdS clusters and silica nanoparticle hybrids [16, 17]. Very recently, graphene-ZnS nanocomposites were successfully prepared by growing the ZnS nanoparticles directly on the graphene oxide nanosheets using a facile two-step wet chemistry process, which exhibit visible light photoactivity towards selective oxidation of alcohols and alkenes under ambient condition [18].

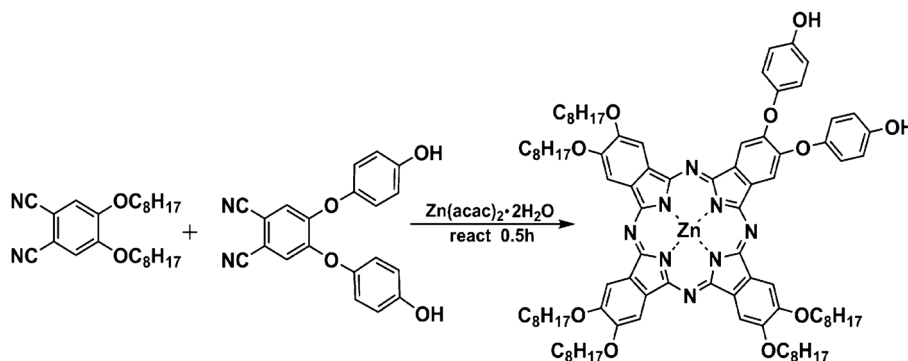
As one of the typical representatives of the functional molecular materials with large conjugated electronic molecular structure, phthalocyanines have been widely applied in flexible display and active-matrix electronic paper as well as smart cards in low-cost memory devices due to their unique optical, electrical, and magnetic properties [19]. The fabrication of ordered nanostructures of these functional molecular materials has also been well studied in the past decade [20–26]. Recently, one-dimensional nanowires of an unsymmetrical phthalocyaninato zinc derivative fabricated

by the interfacial self-assembly were found to display a significantly improved semiconducting properties due to the highly ordered supramolecular structures [27–29]. As part of our continuous effort to construct high-performance phthalocyanine-based semiconducting materials [19b, 19c], herein we describe the synthesis and characterization of an amphiphilic unsymmetrical phthalocyaninato zinc complex, namely 2,3-di(4-hydroxyphenoxy)-9,10,16,17,24,25-hexakis(*n*-octyloxy)phthalocyaninato zinc, Zn[Pc(OC₈H₁₇)₆(OPhOH)₂], Scheme 1. The Langmuir monolayer of this amphiphilic complex has been used as not only an organic template but also the good functional organic material to produce the monodispersed nanoparticles of Zn[Pc(OC₈H₁₇)₆(OPhOH)₂]/ZnS nanocomposite. The organic/inorganic hybrid multilayer films of the Zn[Pc(OC₈H₁₇)₆(OPhOH)₂]/ZnS nanocomposite have also been obtained by depositing monolayers of this amphiphilic complex containing uniformed ZnS nanoparticles using the Langmuir–Shäfer (LS) method. In particular, the resulting Zn[Pc(OC₈H₁₇)₆(OPhOH)₂]/ZnS hybrid film exhibited an remarkably enhanced conductivity relative to the respective single component ones.

RESULTS AND DISCUSSION

Molecular design, synthesis, and electrochemistry

For the purpose of preparing unsymmetrical phthalocyaninato zinc complex with good amphiphilic nature, six hydrophobic octyloxy chains and two hydrophilic hydroxyphenoxy groups were simultaneously introduced onto the periphery of one phthalocyanine chromophore. As shown in Scheme 1, the target 2,3-di(4-hydroxyphenoxy)-9,10,16,17,24,25-hexakis(*n*-octyloxy)phthalocyaninato zinc complex, Zn[Pc(OC₈H₁₇)₆(OPhOH)₂], was synthesized by mixed cyclic tetramerization of 4,5-di(*n*-octyloxy)phthalonitrile and 4,5-di(hydroxyphenoxy)phthalonitrile with the zinc ion as a template [24, 25]. Its matrix-assisted laser desorption/ionization time-of-flight (MALDI-TOF) spectrum showed the molecular ion (M)⁺ signal with



Scheme 1. Synthesis of Zn[Pc(OC₈H₁₇)₆(OPhOH)₂]

correct isotopic pattern, Fig. S1 (Supporting information). The unsymmetrical molecular structure for this novel phthalocyanine compound was unambiguously revealed by its ^1H NMR spectrum. Yield 10 mg (10%). ^1H NMR (CDCl_3 , 400 MHz): δ , ppm 5.32 (12H, t, $-\text{OCH}_2$), 4.83 (12H, m, $-\text{OCH}_2\text{CH}_2$), 3.51 (12H, m, $-\text{OCH}_2\text{CH}_2\text{CH}_2$), 1.59–1.64 (48H, m, $-\text{OCH}_2\text{CH}_2\text{CH}_2(\text{CH}_2)_4$), 0.93–0.97 (18H, m, $-\text{O}(\text{CH}_2)_7\text{CH}_3$), 7.07–7.10 (8H, m, $-\text{OPh}$), 7.02 (2H, s, $-\text{OPhOH}$), 7.54 (2H, s, Ph), 7.88–7.90 (4H, d, Ph), 9.93 (2H, s, Ph). MS (FAB): m/z 1564 (calcd. for $[\text{M} + \text{H}]^+$ 1559.4).

Pressure–area isotherms of the $\text{Zn}[\text{Pc}(\text{OC}_8\text{H}_{17})_6(\text{OPhOH})_2]$ monolayers

Figure 1 shows the reproducible pressure–area (π – A) isotherms of the $\text{Zn}[\text{Pc}(\text{OC}_8\text{H}_{17})_6(\text{OPhOH})_2]$ monolayer on the surfaces of pure water and 0.5 mM ZnSO_4 aqueous solution, respectively, at room temperature. The stable monolayer can be obtained, having limiting molecular area (extrapolated to $\pi = 0$ for condensed region) of 1.52 and 1.69 nm^2 per molecule on the surface of pure water and ZnSO_4 aqueous solution, respectively. These values are slightly bigger than that of the projection for a perpendicular standing molecule of $\text{Zn}[\text{Pc}(\text{OC}_8\text{H}_{17})_6(\text{OPhOH})_2]$ estimated from the minimized structure, Scheme S1 (Supporting information), 1.40 ($3.10 \text{ nm} \times 0.45 \text{ nm}$) $\text{nm}^2/\text{molecule}$, but much smaller than a molecular planar area with a $\text{Zn}[\text{Pc}(\text{OC}_8\text{H}_{17})_6(\text{OPhOH})_2]$ molecule facing on water surface, 8.99 nm^2 ($2.90 \text{ nm} \times 3.10 \text{ nm}$) $\text{nm}^2/\text{molecule}$. An edge-on conformation with the hydrophilic hydroxyphenoxy groups staying close to the water (or ZnSO_4 aqueous solution) surface and the hydrophobic octyloxy chains obliged towards the air phase would then be the most possible orientation of $\text{Zn}[\text{Pc}(\text{OC}_8\text{H}_{17})_6(\text{OPhOH})_2]$ molecules. This is in line with the stacking patterns reported previously for the Langmuir films of substituted phthalocyaninato derivatives [23a, 30]. In addition, the bigger mean molecular

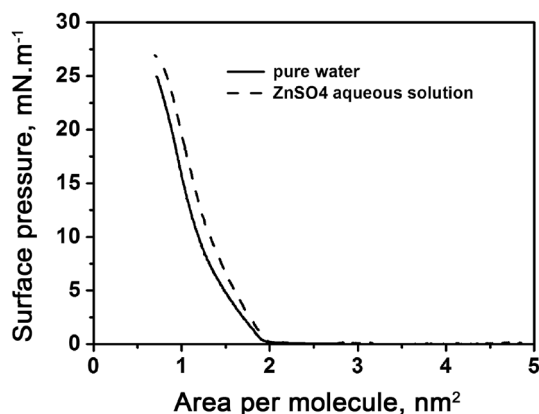


Fig. 1. π – A isotherms for the monolayer of $\text{Zn}[\text{Pc}(\text{OC}_8\text{H}_{17})_6(\text{OPhOH})_2]$ on the surfaces of pure water (solid line) and 0.5 mM ZnSO_4 aqueous solution (dashed line), respectively

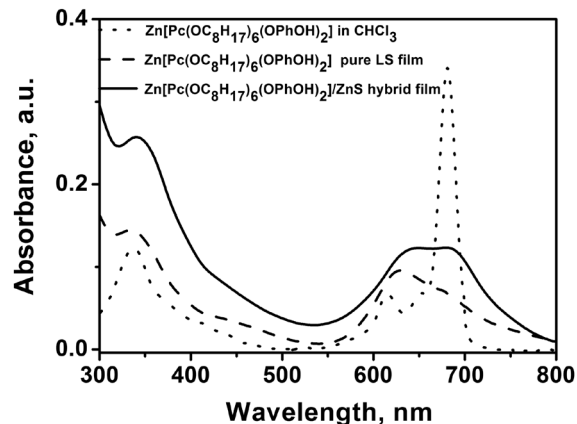


Fig. 2. UV-vis absorption spectra of $\text{Zn}[\text{Pc}(\text{OC}_8\text{H}_{17})_6(\text{OPhOH})_2]$ in CHCl_3 solution (dotted line), $\text{Zn}[\text{Pc}(\text{OC}_8\text{H}_{17})_6(\text{OPhOH})_2]$ pure LS film (dashed line), and $\text{Zn}[\text{Pc}(\text{OC}_8\text{H}_{17})_6(\text{OPhOH})_2]/\text{ZnS}$ hybrid film (solid line)

area (1.69 nm^2 per molecule) of $\text{Zn}[\text{Pc}(\text{OC}_8\text{H}_{17})_6(\text{OPhOH})_2]$ on ZnSO_4 aqueous solution than that on the pure water subphase (1.52 nm^2 per molecule) suggested the stronger interaction between the $\text{Zn}[\text{Pc}(\text{OC}_8\text{H}_{17})_6(\text{OPhOH})_2]$ molecules and the Zn^{2+} subphase.

UV-vis absorption spectra

Figure 2 compares the UV-vis absorption spectra of $\text{Zn}[\text{Pc}(\text{OC}_8\text{H}_{17})_6(\text{OPhOH})_2]$ in chloroform solution and in the pure LS film as well as $\text{Zn}[\text{Pc}(\text{OC}_8\text{H}_{17})_6(\text{OPhOH})_2]/\text{ZnS}$ hybrid film. The absorption spectrum of $\text{Zn}[\text{Pc}(\text{OC}_8\text{H}_{17})_6(\text{OPhOH})_2]$ in chloroform solution displays a typical Soret band at 337 nm and the main Q-band at 681 nm with the vibrational shoulder at 615 nm, in line with the previous reports for monomeric phthalocyaninato metal complexes [31, 32]. However, after being fabricated into the pure LS film, the main Q-band is broadened and blue shifted from 681 to 622 nm, Fig. 2, indicating the formation of H aggregates in the multilayer films due to the strong π – π interaction between phthalocyanine molecules [31, 33]. By comparing the electronic absorption spectra of the $\text{Zn}[\text{Pc}(\text{OC}_8\text{H}_{17})_6(\text{OPhOH})_2]/\text{ZnS}$ hybrid film and the pure LS film, Fig. 2, one can see that the $\text{Zn}[\text{Pc}(\text{OC}_8\text{H}_{17})_6(\text{OPhOH})_2]/\text{ZnS}$ hybrid film exhibits a higher absorption intensity in the wavelength region below 400 nm, very similar to the absorption of nanosized ZnS particles on the graphene sheet [18]. However, the main Q-band of $\text{Zn}[\text{Pc}(\text{OC}_8\text{H}_{17})_6(\text{OPhOH})_2]$ in the hybrid film still showed a blue-shift from 681 nm to 662 [(637 + 687)/2] nm, suggesting the similar packing behavior of $\text{Zn}[\text{Pc}(\text{OC}_8\text{H}_{17})_6(\text{OPhOH})_2]$ molecules in both pure and hybrid film. It is worth noting that the more marked shift in the pure LS film than that in the hybrid film indicates that a stronger intermolecular interaction for the $\text{Zn}[\text{Pc}(\text{OC}_8\text{H}_{17})_6(\text{OPhOH})_2]$ molecules existed in pure film than that in the hybrid one. This in turn suggests the significant effect of the ZnS nanoparticles on the

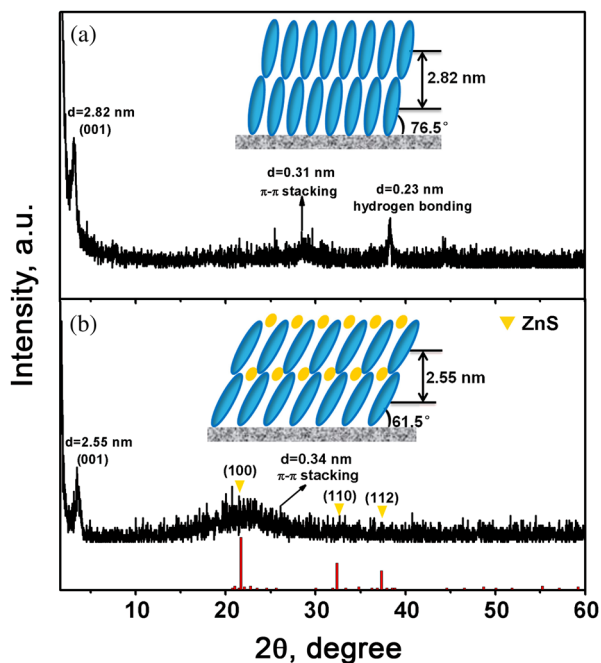


Fig. 3. X-ray patterns for the LS films of $\text{Zn}[\text{Pc}(\text{OC}_8\text{H}_{17})_6(\text{OPhOH})_2]$ (a) and $\text{Zn}[\text{Pc}(\text{OC}_8\text{H}_{17})_6(\text{OPhOH})_2]/\text{ZnS}$ (b) deposited on SiO_2 substrate. The insets are the schematic packing modes of the $\text{Zn}[\text{Pc}(\text{OC}_8\text{H}_{17})_6(\text{OPhOH})_2]$ molecules in pure LS film and hybrid film, respectively. The insets are schematic packing modes of the $\text{Zn}[\text{Pc}(\text{OC}_8\text{H}_{17})_6(\text{OPhOH})_2]$ pure LS film and $\text{Zn}[\text{Pc}(\text{OC}_8\text{H}_{17})_6(\text{OPhOH})_2]/\text{ZnS}$ hybrid film

intermolecular interaction of $\text{Zn}[\text{Pc}(\text{OC}_8\text{H}_{17})_6(\text{OPhOH})_2]$ molecules in the hybrid film, which is in accordance with the conclusion deduced from the XRD studies as detailed below.

X-ray diffraction patterns

The internal structures of $\text{Zn}[\text{Pc}(\text{OC}_8\text{H}_{17})_6(\text{OPhOH})_2]$ and $\text{Zn}[\text{Pc}(\text{OC}_8\text{H}_{17})_6(\text{OPhOH})_2]/\text{ZnS}$ LS films are further assessed using the out-of-plane (OOP) X-ray diffraction (XRD) technique. As shown in Figs 3a and 3b, in the low-angle range, the XRD patterns of both pure $\text{Zn}[\text{Pc}(\text{OC}_8\text{H}_{17})_6(\text{OPhOH})_2]$ film and $\text{Zn}[\text{Pc}(\text{OC}_8\text{H}_{17})_6(\text{OPhOH})_2]/\text{ZnS}$ hybrid film exhibit the (001) Bragg peak at $2\theta = 3.14^\circ$ and 3.46° , respectively, corresponding to a periodic spacing distance of 2.82 and 2.55 nm for $\text{Zn}[\text{Pc}(\text{OC}_8\text{H}_{17})_6(\text{OPhOH})_2]$ molecules in the solid films, respectively. Consequently, orientation angles of the Pc ring with respect to the substrate surface of *ca.* 76.5° and 61.5° are estimated, respectively, for $\text{Zn}[\text{Pc}(\text{OC}_8\text{H}_{17})_6(\text{OPhOH})_2]$ in pure and composite films based on the width of $\text{Zn}[\text{Pc}(\text{OC}_8\text{H}_{17})_6(\text{OPhOH})_2]$ (2.9 nm) taken from the energy-optimized molecular structure, Scheme S1 (Supporting information). A slipped co-facial stacking mode with an “edge-on” configuration (*H* aggregate) on the surface of the substrate was then achieved for $\text{Zn}[\text{Pc}(\text{OC}_8\text{H}_{17})_6(\text{OPhOH})_2]$ in either pure

or composite film (as shown in the insets of Fig. 3) [28]. This is in line with the UV-vis absorption result. It is worth noting that a slightly smaller monolayer thickness of $\text{Zn}[\text{Pc}(\text{OC}_8\text{H}_{17})_6(\text{OPhOH})_2]$ in the $\text{Zn}[\text{Pc}(\text{OC}_8\text{H}_{17})_6(\text{OPhOH})_2]/\text{ZnS}$ hybrid film than that in the pure film should be attributed to a greater planar conformation of the Pc molecule in the composite film, which is in agreement with the experimental observation of the π -A isotherms. Furthermore, these results also indicate that the orientation and packing model of $\text{Zn}[\text{Pc}(\text{OC}_8\text{H}_{17})_6(\text{OPhOH})_2]$ molecules are determined primarily at the air-water interface, which do not change significantly from the water surface to the solid substrates. This result is in line with the findings reported previously [31]. In addition, in the wide angle region, the OOP XRD pattern of pure $\text{Zn}[\text{Pc}(\text{OC}_8\text{H}_{17})_6(\text{OPhOH})_2]$ LS film, Fig. 3a, presents two diffractions at 0.31 and 0.23 nm, respectively, which can be attributed to the distance of π - π stacking distance from Pc rings between the adjacent $\text{Zn}[\text{Pc}(\text{OC}_8\text{H}_{17})_6(\text{OPhOH})_2]$ molecules and the distance between hydrogen-bonding hydroxyl oxygens [27, 32–34]. However, in the 2θ range of 20° – 60° , the OOP XRD pattern of the $\text{Zn}[\text{Pc}(\text{OC}_8\text{H}_{17})_6(\text{OPhOH})_2]/\text{ZnS}$ hybrid film exhibited three diffraction peaks, which were assigned to the (100), (110), and (112) planes of the hexagonal phase of wurtzite ZnS for the nanoparticles formed on the $\text{Zn}[\text{Pc}(\text{OC}_8\text{H}_{17})_6(\text{OPhOH})_2]$ film, according to JCPDS file no. 12-0688, Fig. 3b. Nevertheless, no diffraction from the hydrogen-bonding between hydroxyphenoxy groups of $\text{Zn}[\text{Pc}(\text{OC}_8\text{H}_{17})_6(\text{OPhOH})_2]$ molecules was detected in the $\text{Zn}[\text{Pc}(\text{OC}_8\text{H}_{17})_6(\text{OPhOH})_2]/\text{ZnS}$ hybrid film, while an increased distance from π - π stacking at 0.34 nm between adjacent Pc rings of $\text{Zn}[\text{Pc}(\text{OC}_8\text{H}_{17})_6(\text{OPhOH})_2]$ molecules was observed, in comparison with that for the pure $\text{Zn}[\text{Pc}(\text{OC}_8\text{H}_{17})_6(\text{OPhOH})_2]$ LS film. This again suggests the obvious influence of the ZnS nanoparticles grown on the organic template to the assembly structure of $\text{Zn}[\text{Pc}(\text{OC}_8\text{H}_{17})_6(\text{OPhOH})_2]$ molecules in the hybrid film. The OOP XRD patterns in combination with AFM analysis of the samples provided exclusive evidence for the formation of the ZnS nanoparticles in the $\text{Zn}[\text{Pc}(\text{OC}_8\text{H}_{17})_6(\text{OPhOH})_2]$ film (*vide infra*).

Morphology

The surface morphologies of $\text{Zn}[\text{Pc}(\text{OC}_8\text{H}_{17})_6(\text{OPhOH})_2]$ pure LS film and $\text{Zn}[\text{Pc}(\text{OC}_8\text{H}_{17})_6(\text{OPhOH})_2]/\text{ZnS}$ hybrid film were examined by atomic force microscope (AFM). As revealed in Fig. 4, depending on the hydrogen bonding and intermolecular π - π interaction among neighboring phthalocyanine molecules, the $\text{Zn}[\text{Pc}(\text{OC}_8\text{H}_{17})_6(\text{OPhOH})_2]$ LS film prepared from the surface of pure water results in the unique reticular-like nanostructures with *ca.* 550 nm in length and 140 nm in width, giving a root mean square (rms) roughness value of 12.8 nm, Fig. 4a. After the formation of ZnS nanostructures on the $\text{Zn}[\text{Pc}(\text{OC}_8\text{H}_{17})_6(\text{OPhOH})_2]$ film, the resulting $\text{Zn}[\text{Pc}(\text{OC}_8\text{H}_{17})_6(\text{OPhOH})_2]/\text{ZnS}$ hybrid

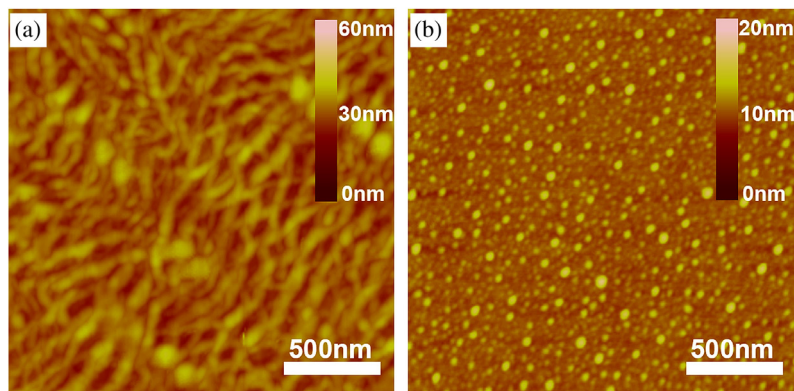


Fig. 4. AFM images of Zn[Pc(OC₈H₁₇)₆(OPhOH)₂] pure LS film (a) and Zn[Pc(OC₈H₁₇)₆(OPhOH)₂]/ZnS hybrid film (b) on HMDS-treated Si/SiO₂ substrate

film exhibits a granular nanostructure with uniform grain crystallites and the average diameter of *ca.* 65 nm, Fig. 4b. A rms roughness value of 2.67 nm is achieved, typical of a particularly smooth surface film-structure without large grain boundaries. The more uniform grain size, much lower rms value, and higher grain crystallinity for the Zn[Pc(OC₈H₁₇)₆(OPhOH)₂]/ZnS hybrid film in comparison with those of Zn[Pc(OC₈H₁₇)₆(OPhOH)₂] pure LS film are expected to induce fewer traps and/or defects localized around the grain boundaries, which in turn becomes responsible for the improved carrier mobility of the former hybrid film [35, 36].

I–V properties

The semiconducting properties of both Zn[Pc(OC₈H₁₇)₆(OPhOH)₂] pure LS film and Zn[Pc(OC₈H₁₇)₆(OPhOH)₂]/ZnS hybrid film were investigated by current–voltage (I–V) measurements, Fig. 5. According to the equation reported in the literatures [37, 38], the electrical conductivity of Zn[Pc(OC₈H₁₇)₆(OPhOH)₂]/ZnS hybrid film extracted from the quasilinear region at low bias (up to 40 V) was estimated to amount to around $3.78 \times 10^{-6} \text{ S.cm}^{-1}$, which is more than *ca.* 1 order of magnitude larger than that of the Zn[Pc(OC₈H₁₇)₆(OPhOH)₂] pure LS film with the value of *ca.* $2.87 \times 10^{-7} \text{ S.cm}^{-1}$ and three orders of magnitude larger than that of the bulk ZnS crystals ($\sim 10^{-9} \text{ S.cm}^{-1}$) [39] (it is noteworthy that the I–V measurement experiments were repeated for more than three times on different pieces of films). Obviously, the Zn[Pc(OC₈H₁₇)₆(OPhOH)₂]/ZnS hybrid film displays a significantly enhanced conductivity relative to that of either the bulk ZnS crystals or pure Zn[Pc(OC₈H₁₇)₆(OPhOH)₂] LS film due not only to the higher film quality (more uniform grain size, much lower R_{rms} value, and higher crystallinity) for carrier transport in the hybrid film but more importantly to the existence of the densely packed molecular architecture of the Zn[Pc(OC₈H₁₇)₆(OPhOH)₂] and ZnS nanoparticles

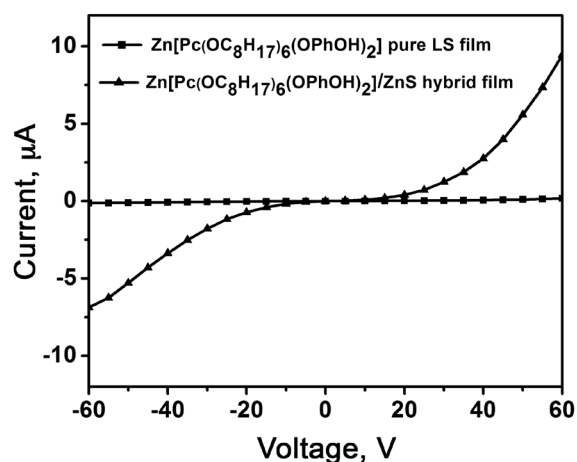


Fig. 5. I–V curves measured for the Zn[Pc(OC₈H₁₇)₆(OPhOH)₂] pure LS film (■) and Zn[Pc(OC₈H₁₇)₆(OPhOH)₂]/ZnS hybrid film (▲) deposited on ITO IDEs/glass substrate, respectively

(as dopants) in the film matrix that would be easier for creation of charge carriers.

EXPERIMENTAL

Chemicals and measurements

All solvents were dried and distilled according to standard procedures. All other solvents and reagents such as Zn(OAc)₂·2H₂O were used as received. All air-sensitive reactions were carried out within nitrogen-filled space. *N,N*-dimethylformamide (DMF) and dichloromethane (CH₂Cl₂) were freshly distilled just before use. Column chromatography was carried out on silica gel (Merck, Kieselgel 60, 200–300 mesh) with the indicated eluent. 2,3-di(4-hydroxyphenoxy)-9,10,16,17,24,25-hexakis-(*n*-octyloxy)phthalocyaninato zinc complex, Zn[Pc(OC₈H₁₇)₆(OPhOH)₂], was synthesized and purified according to the published procedure [24, 25].

NMR spectra were recorded with Bruker Avance 400 spectrometer at 298 K using partially deuterated solvents as internal standards. Chemical shifts (δ) are denoted in ppm. Electronic absorption spectra were recorded on a Hitachi U-4100 spectrophotometer. X-ray diffraction experiment was carried out on a Bruker D8 FOCUS X-ray diffractometer. AFM images were collected under ambient conditions using the tapping mode with a NanoscopeIII/Bioscope scanning probe microscope from Digital instruments.

Synthesis of Zn[Pc(OC₈H₁₇)₆(OPhOH)₂]

A mixture of 4,5-di(*n*-octyloxy)phthalonitrile (0.201 mmol, 77.2 mg), 4,5-di(hydroxyphenoxy)phthalonitrile (0.067 mmol, 23.0 mg), Zn(acac)₂·2H₂O (0.168 mmol, 37.0 mg) in dry *n*-octanol (2.0 mL) were heated to 250 °C for 0.5 h under N₂ atmosphere. After being cooled to room temperature, the residue left was chromatographed on a silica gel column with CHCl₃/CH₃OH as eluent. Repeated chromatography followed by recrystallization from CHCl₃ and methanol gave pure compound as a green powder.

Formation of the nanocomposite and the preparation of pure and hybrid films

An aqueous solution of ZnSO₄ (5×10^{-4} M, pH = 5.5) in ultrapure water with resistivity greater than 18 M Ω .cm⁻¹ was used as the subphase. A beaker filled with the subphase and the Na₂S aqueous solution that was used to produce H₂S gas, respectively, were placed in a sealed 7.8 L container. The Langmuir monolayer of Zn[Pc(OC₈H₁₇)₆(OPhOH)₂] was formed by spreading 5 μ L 5×10^{-4} M Zn[Pc(OC₈H₁₇)₆(OPhOH)₂] chloroform solution onto the 5×10^{-4} M ZnSO₄ aqueous solution surface of 25.6 cm². The mean molecular area was calculated to be 1.70 nm², which corresponds to the molecular area obtained by the π -A isotherm from Langmuir trough (NIMA 622, Great Britain). After evaporating the organic solvent for 15 min, H₂SO₄ was poured into the Na₂S aqueous solution to produce H₂S and the container was sealed immediately. After a reaction time of 30 min, the monolayer was transferred onto Si/SiO₂ and quartz slides, respectively, by the Langmuir–Shäfer (LS: horizontal transfer) method for AFM, X-ray diffraction, UV-vis and I–V measurements. The pure LS film was obtained by depositing monolayers of the amphiphilic complex at a constant surface pressure of 20 mN.m⁻¹ by using the LS method.

Device fabrication

The fundamental electrical measurements were performed using a Hewlett-Packard (HP) 4140B parameter analyzer at room temperature. I–V curves were registered in the -60 to 60 V voltage range with 5 V increments, starting and finishing at 0 V bias to avoid irreversible polarization effects. All experiments have been conducted

at least twice to ensure the reproducibility. A 20 nm-thick gold interdigitated electrode (IDE) array composed of 6 pairs of Au electrode digits was deposited on a SiO₂/Si substrate *via* a shadow mask. The interelectrode spacing and overlapping length of the IDE were 0.24 and 2.60 mm, respectively. Zn[Pc(OC₈H₁₇)₆(OPhOH)₂] pure and Zn[Pc(OC₈H₁₇)₆(OPhOH)₂]/ZnS hybrid LS films were deposited on Si/SiO₂ substrate consisting of gold IDEs for the I–V measurements. The conductivity, σ , can be calculated according to the equation reported in the previous literatures [37, 38].

CONCLUSION

Briefly summarizing above, a new unsymmetrical amphiphilic phthalocyaninato zinc complex has been designed and synthesized. This amphiphilic Zn[Pc(OC₈H₁₇)₆(OPhOH)₂] complex can form stable Langmuir monolayer on the surface of both water and ZnSO₄ aqueous solution. By using the Langmuir monolayer of Zn[Pc(OC₈H₁₇)₆(OPhOH)₂] as an organic template, highly uniform ZnS–Zn[Pc(OC₈H₁₇)₆(OPhOH)₂] hybrid nanoparticles were prepared. Surface pressure-area isotherms, UV-vis spectroscopy, and XRD studies indicate that the Zn[Pc(OC₈H₁₇)₆(OPhOH)₂] molecules adopt a face-to-face configuration and edge-on orientation in both the pure LS film and Zn[Pc(OC₈H₁₇)₆(OPhOH)₂]/ZnS hybrid film. Furthermore, comparing to pure LS film (with conductivity 2.87×10^{-7} S.cm⁻¹) or bulk ZnS crystals (with conductivity $\sim 10^{-9}$ S.cm⁻¹), Zn[Pc(OC₈H₁₇)₆(OPhOH)₂]/ZnS hybrid film has a significantly larger conductivity (3.78×10^{-6} S.cm⁻¹). The result achieved is certainly helpful for the development of new organic-inorganic composite nanostructures with tunable functionality, which may be applied in a wide range of electronic and sensor devices.

Acknowledgments

This work was financially supported by the Natural Science Foundation of China (nos. 21371073 and 21290174), the National Key Basic Research Program of China (nos. 2013CB933402 and 2012CB224801).

Supporting information

Figure S1 and Scheme S1 are given in the supplementary material. This material is available free of charge *via* the Internet at <http://www.worldscinet.com/jpp/jpp.shtml>.

REFERENCES

1. Bi W, Louvain N, Mercier N, Luc J, Rau I, Kajzar F and Sahraoui B. *Adv. Mater.* 2008; **20**: 1013–1017.
2. Kagan CR, Mitzi DB and Dimitrakopoulos CD. *Science* 1999; **286**: 945–947.

3. Kira A, Umeyama T, Matano Y, Yoshida K, Isoda S, Isosomppi M, Tkachenko NV, Lemmetyinen H and Imahori H. *Langmuir* 2006; **22**: 5497–5503.
4. Nishimura A, Sagawa N and Uchino T. *J. Phys. Chem. C* 2009; **113**: 4260–4262.
5. (a) Hu L, Zhao Y-L, Ryu K, Zhou C, Stoddart JF and Grüner G. *Adv. Mater.* 2008; **20**: 939–946. (b) Hao E-C, Wang L-Y, Zhang J-H, Yang B, Zhang X and Shen J-C. *Chem. Lett.* 1999; **1**: 5–6.
6. (a) Sheeney-Haj-Ichia L, Basnar B and Willner I. *Angew. Chem., Int. Ed.* 2005; **44**: 78–83. (b) Kotov NA, Dekany I and Fendler JH. *J. Phys. Chem.* 1995; **99**: 13065–13069.
7. (a) Rella R, Rizzo A, Licciulli A, Siciliano P, Troisi L and Valli L. *Mater. Sci. Engineer C* 2002; **22**: 439–443. (b) Serra A, Genga A, Manno D, Micocci G, Siciliano T and Tepore A. *Langmuir* 2003; **19**: 3486–3492.
8. Chen Y-L, Chen L-N, Qi G-J, Wu H-X, Zhang Y-X, Xue L, Zhu P-H, Ma P and Li X-Y. *Langmuir* 2010; **26**: 12473–12478.
9. Song J-G, Tian Q-W, Gao J, Wu H-X, Chen Y-L and Li X-Y. *CrystEngComm* 2014; **16**: 1277–1286.
10. Vilan A and Cahen D. *Trends Biotechnol.* 2002; **20**: 22–29.
11. Van Bommel KJC, Friggeri A and Shinkai S. *Angew. Chem., Int. Ed.* 2003; **42**: 980–999.
12. Lu Y-F, Yang Y, Sellinger A, Lu M-C, Huang J-M, Fan H-Y, Haddad R, Lopez G, Burns AR, Sasaki DY, Shelnut J and Brinker CJ. *Nature* 2001; **410**: 913–917.
13. (a) Valli L. *Adv. Colloid Interface Sci.* 2005; **116**: 13–44. (b) Bettini S, Pagano R, Bonfrate V, Maglie E, Manno D, Serra A, Valli L and Giancane G. *J. Phys. Chem. C* 2015; **119**: 20143–20149.
14. Sone ED, Zubarev ER and Stupp SI. *Angew. Chem. Int. Ed.* 2002; **41**: 1705–1709.
15. Chen C-C and Lin J-J. *Adv. Mater.* 2001; **13**: 136–139.
16. Liu L-Q, Wang T-X, Li J-X, Guo Z-X, Dai L-M, Zhang D-Q and Zhu D-B. *Chem. Phys. Lett.* 2003; **367**: 747–752.
17. Li X-L, Liu Y-Q, Fu L, Cao L-C, Wei D-C and Wang Y. *Adv. Funct. Mater.* 2006; **16**: 2431–2437.
18. (a) Wang P, Jiang T-F, Zhu C-Z, Zhai Y-M, Wang D-J and Dong S-J. *Nano Research* 2010; **3**: 794–799. (b) Zhang Y-H, Zhang N, Tang Z-R and Xu Y-J. *ACS Nano* 2012; **6**: 9777–9789.
19. (a) Horowitz G. *Adv. Mater.* 1998; **10**: 365–377. (b) Kan J-L, Chen Y-L, Qi D, Liu Y-Q and Jiang J-Z. *Adv. Mater.* 2012; **24**: 1755–1758. (c) Kong X, Zhang X, Gao D-M, Qi D-D, Chen Y-L and Jiang J-Z. *Chem. Sci.* 2015; **6**: 1967–1972. (d) Kong X, Jia Q, Wu F-H and Chen Y-L. *Dyes Pigm.* 2015; **115**: 67–72. (e) Katz HE, Bao Z-N and Gilat SL. *Acc. Chem. Res.* 2001; **34**: 359–369. (f) Würthner F. *Angew. Chem. Int. Ed.* 2001; **40**: 1037–1039. (g) Dimitrakopoulos CD and Malenfant PRL. *Adv. Mater.* 2002; **14**: 99–117. (h) Jiang J-Z and Ng DKP. *Acc. Chem. Res.* 2009; **42**: 79–88. (i) Sun Y-M, Liu Y-Q and Zhu D-B. *J. Mater. Chem.* 2005; **15**: 53–65. (j) Sirringhaus H. *Adv. Mater.* 2005; **17**: 2411–2425.
20. (a) Rosenthal I and Ben-Hur E. *Int. J. Radiat. Biol.* 1995; **67**: 85–91. (b) Bonnett R. *Chem. Soc. Rev.* 1995; **24**: 19–33.
21. (a) Gregory P. *High-Technology Applications of Organic Colorants*, Plenum Press: New York, 1991. (b) Ao R, Kilmert L and Haarer D. *Adv. Mater.* 1995; **7**: 495–499. (c) Birkett D. *Chem. Ind.* 2000; **5**: 178–181.
22. Lu G, Chen Y-L, Zhang X, Bao M, Bian Y-Z, Li X-Y and Jiang J-Z. *J. Am. Chem. Soc.* 2008; **130**: 11623–11630.
23. (a) Chen Y-L, Su W, Bai M, Jiang J-Z, Li X-Y, Liu Y-Q, Wang L-X and Wang S-Q. *J. Am. Chem. Soc.* 2005; **127**: 15700–15701. (b) Bouvet M and Pauly A. *Molecular-based Gas Sensors, the Encyclopedia of Sensors*, Vol. 6, Grimes CA, Dickey EC and Pishko MV. (Eds.) American Scientific Publishers: Valencia, CA. 2006; pp. 227–270. (c) Zhang Y-X, Cai X, Bian Y-Z and Jiang J-Z. *Struct. Bond.* 2010; **135**: 275–322. (d) Zhang X, Gao D-M, Gao J, Zhu P-H, Bouvet M and Chen Y-L. *RSC Adv.* 2014; **4**: 14807–14814.
24. Liu W, Jiang J-Z, Du D-M and Arnold DP. *Aust. J. Chem.* 2000; **53**: 131–136.
25. Maree SE and Nyokong T. *J. Porphyrins Phthalocyanines* 2001; **5**: 782–792.
26. Chen Y-L, Bouvet M, Sizun T, Gao Y-N, Plassard C, Lesniewska E and Jiang J-Z. *Phys. Chem. Chem. Phys.* 2010; **12**: 12851–12861.
27. Ma P, Bai Z-P, Gao Y-N, Wang Q-B, Kan J-L, Bian Y-Z and Jiang J-Z. *Soft Matter* 2011; **7**: 3417–3422.
28. (a) Zhang Y-X, Zhang X-X, Liu Z-Q, Bian Y-Z and Jiang J-Z. *J. Phys. Chem. A* 2005; **109**: 6363–6370. (b) Kasha M, Rawls HR and El-Bayoumi MA. *Pure Appl. Chem.* 1965; **11**: 371–392.
29. (a) Li R-J, Zhang X-X, Zhu P-H, Ng DKP, Kobayashi N and Jiang J-Z. *Inorg. Chem.* 2006; **45**: 2327–2334; (b) Bian Y-Z, Li L, Dou J-M, Cheng DYY, Li R-J, Ma C-Q, Ng DKP, Kobayashi N and Jiang J-Z. *Inorg. Chem.* 2004; **43**: 7539–7544. (c) Chen Y-L, Bouvet M, Sizun T, Barochi G, Rossignol J and Lesniewska E. *Sens. Actuators B.* 2011; **155**: 165–173.
30. (a) Chen Y-L, Li R-J, Wang R-M, Ma P, Dong S, Gao Y-N, Li X-Y and Jiang J-Z. *Langmuir* 2007; **23**: 12549–12554. (b) Liu H-G, Qian D-J, Feng X-S, Xue Q-B and Yang K-Z. *Langmuir* 2000; **16**: 5079–5085. (c) Schick GA, Schreiman IC, Wagner RW, Jonathan SL and David FB. *J. Am. Chem. Soc.* 1989; **111**: 1344–1350. (d) Kroon JM, Sudhoelter EJR, Schenning APHJ and Nolteet RJM. *Langmuir* 1995; **11**: 214–220.

31. Chen Y-L, Liu H-G, Zhu P-H, Zhang Y, Wang X-Y, Li X-Y and Jiang J-Z. *Langmuir* 2005; **21**: 11289–11295.
32. Janczak J and Idemori YM. *Inorg. Chem.* 2002; **41**: 5059–5065.
33. Gardberg AS, Yang S, Hoffman BM and Ibers JA. *Inorg. Chem.* 2002; **41**: 1778–1781.
34. Kimura M, Muto T, Takimoto H, Wada K, Ohta K, Hanabusa K, Shirai H and Kobayashi N. *Langmuir* 2000; **16**: 2078–2086.
35. Durban MM, Kazarinoff PD and Luscombe CK. *Macromolecules* 2010; **43**: 6348–6352.
36. Lee T, Landis CA, Dhar BM, Jung BJ, Sun J, Sarjeant A, Lee HJ and Katz HE. *J. Am. Chem. Soc.* 2009; **131**: 1692–1705.
37. Chen Y-L, Li D-P, Yuan N, Gao J, Gu R-M, Lu G-F and Bouvet M. *J. Mater. Chem.* 2012; **22**: 22142–22149.
38. (a) Derouiche H, Bernede JC and Hyver JL. *Dyes Pigm.* 2004; **53**: 277–289. (b) Xie B, Finstad CC and Muscat AJ. *Chem. Mater.* 2005; **17**: 1753–1764. (c) Lu G, Zhang X, Cai X and Jiang J-Z. *J. Mater. Chem.* 2009; **19**: 2417–2424.
39. Abdulkhadar M and Thomas B. *Nanostruct. Mater.* 1998; **10**: 593–600.